Operational Assistance System using 3-DOF Joystick with Reaction Force Display to Load Transfer Machine in a Plane

Tomoya Kuneguchi[1], Yoshiyuki Noda[1], Yukinori Sago[2] and Kiyoaki Kakihara[3]
[1]*Department of Mechanical Systems Engineering, University of Yamanashi, Takeda 4-3-11, Kofu, Japan*
[2]*Department of Mechanical Engineering, Toyohashi University of Technology, Toyohashi, Japan*
[3]*KER Co., Ltd, Toyokawa, Japan*

Keywords: Operational assistance, load transfer machine, 3-DOF Joystick, Reaction Force Display, Obstacles Avoidance.

Abstract: This paper is concerned with an operational assistance system to a load transfer machine in a plane such as a manually guided vehicle and a crane without vertical transfer. In the transfer machine, collisions with obstacles are often occurred by the incorrect operations. Therefore, in order to avoid the obstacles to the transfer machine, the operational assistance system using 3-DOF(3 Degree of Freedom) joystick with reaction force display is proposed in this study. The 3-DOF joystick enables operator to manipulate the transfer machine with back-and-forth, left-and-right, and rotation motions. And, it has motors for presenting the reaction force on each axis. In this system, the joystick displays the reaction force which consists of the virtual elastic force and viscosity resistance, which are controlled by PD control gains. By associating the gains in the PD control with the distance between the obstacles and the transfer object, the joystick operation is constrained for avoiding the obstacles. The effectiveness of the proposed operational assistance system is verified by the experiments using the simulator of the transfer machine manipulated by the 3-DOF joystick.

1 INTRODUCTION

A load transfer machine such as a crane and an industrial vehicle is widely used in industry. It is required to transfer the load efficiently(Sawodny, Aschemann and Lahres, 2002), (Osumi, Kubo, Yano and Saito, 2010). However, since there are some obstacles in the transfer space, the operator has to manipulate the transfer machine to avoid the obstacles. The skill is required to manipulate the transfer machine. However, even if the skilled worker operates the transfer machine, the collisions with the obstacles are often occurred by the incorrect operation. 30 fatal accidents by cranes occurred in Japan in 2011, of which fifteen were the accidents by the incorrect operation(Japan Crane Association, 2011). Including the unreported accidents such as a near-miss accident, there are a lot of accidents by the incorrect operation in the transfer machines.

In order to operate safety the crane, some operational assistance systems have been proposed in the previous studies. The sway of the load in the crane is occurred by the inappropriate operation. For suppressing the sway of the load, the operational assistance system with the haptic device was proposed(Yoneda, Arai, Fukuda and Miyata, 1999). The crane operation assistance system using the augmented reality technology was proposed in the study(Yi-Chen, Hung-Lin, Shin-Chung and Shang-Hsien, 2011). In this system, the actual information of the working environment and the virtual information such as building information are integrated and displayed on the monitor. However, the operational assistance systems for avoiding the obstacles have not been proposed in most previous studies as seen from the above. In one of the previous studies, the operational assistance system for avoiding the obstacles using the haptic joystick was proposed(Sato, Noda, et.al., 2009). However, since the overall size of the transfer object has not been considered in the system, the collision of the obstacles and the edge of the transfer object might be occurred. Moreover, the design method of the parameters in the joystick control system are unclear in the paper. It is desired to design clearly the operational assistance system using the haptic joystick with consideration of the overall size of the transfer object for obstacles avoidance.

Recently, an omnidirectional mobile vehicle has been developed as a next-generation personal vehicle(Noda, Kawaguchi and Terashima, 2010). This

Kuneguchi T., Noda Y., Sago Y. and Kakihara K..
Operational Assistance System using 3-DOF Joystick with Reaction Force Display to Load Transfer Machine in a Plane.
DOI: 10.5220/0005026303460352
In *Proceedings of the 11th International Conference on Informatics in Control, Automation and Robotics* (ICINCO-2014), pages 346-352
ISBN: 978-989-758-040-6

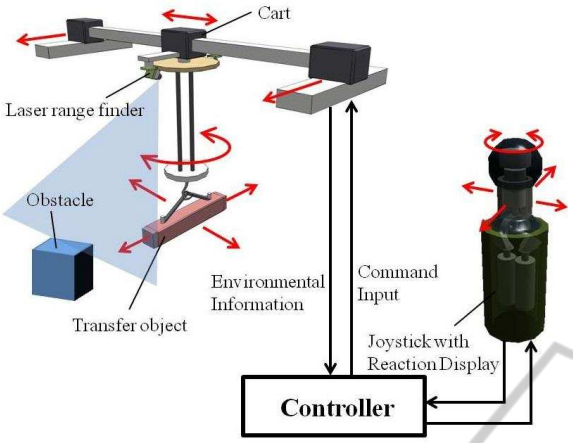

Figure 1: Crane system manipulated by 3-DOF joystick.

vehicle has 3-DOF motion with back-and-forth, left-and-right, and rotation. However in the previous studies, the vehicle has been operated by the 2-DOF joystick and switching equipment which switches between the lateral and the rotation motions. Therefore, it cannot be transferred freely in a plane. For improving the operability of the vehicle, 3-DOF operation device is required. On the other hand, the incorrect operation will be increased by applying the 3-DOF joystick. The operation device with high operability and safety is demanded for the useful transfer machine with high degree of freedom motion.

Therefore, the present authors are developing the operational assistance system using 3-DOF joystick with reaction force display for the load transfer machine. The example of the application of the developing operational assistance system is shown in Figure 1. In Figure 1, the operational assistance system is integrated into the overhead traveling crane system. The crane system has 3-DOF transfer with back-and-forth, left-and-right, and rotation. In order to avoid the obstacles, the joystick operation is constrained dynamically by the reaction force display.

In this paper, 3-DOF joystick with the reaction force displayed on each axis is proposed. In order to constrain dynamically the joystick operation for the obstacle avoidance, about 30[N] of the maximum reaction force can be generated by the servomotors installed the joystick. Moreover, the operational assistance system using the 3-DOF joystick is proposed for operating the machine freely and safety. In this system, the joystick displays the reaction force which consists of the virtual elastic force and viscosity resistance controlled by PD control gains. Furthermore, by associating the gains in the PD control with the distance between the obstacles and the transfer object, the joystick operation is constrained for avoiding the

Figure 2: Photo of 3-DOF joystick.

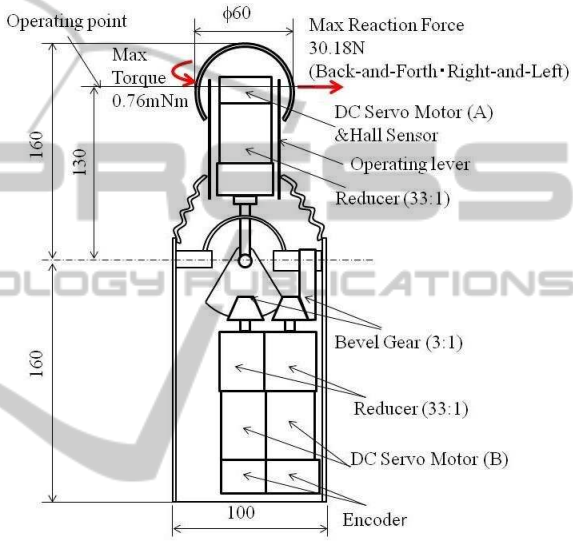

Figure 3: Schematic view of 3-DOF joystick structure.

Table 1: Specifications of DC servomotors.

	Rating Torque	Rating Current
DC Motor (A)	23.3[mNm]	0.49[A]
DC Motor (B)	33.6[mNm]	1.48[A]

obstacles.

The effectiveness of the proposed operational assistance system is verified by the experiments using the simulator of the transfer machine manipulated by the 3-DOF joystick.

2 3-DOF JOYSTICK

The photo and the schematic view of the 3-DOF joystick proposed in this study are shown in Figures 2 and 3, respectively. This joystick has three servomotors, and can provide the reaction force to operation of back-and-forth, left-and-right, and rotation as shown in Figure 3. The specifications of the installed motors in the joystick are shown in Table 1. The reaction force to the back-and-forth operation can be displayed

by increasing the driving torque of the motor through the reducer and the bevel gear. The reaction force to the left-and-right operation also can be displayed by the same structure with the back-and-forth operation. The tilting angle of the operating lever can be detected by the rotary encoders attached to the motors. The motor for displaying the reaction force to the rotation operation is installed into the operating lever. The reaction force can be displayed by self-rotating the motor with the reducer. The rotating angle of the operating lever can be detected by the hall sensor installed into the motor. The maximum reaction forces at the operation point to the back-and-forth and the left-and-right operations are 30.18[N]. The maximum reaction torque to the rotation operation is 0.76[mNm]. They are sufficient to constrain the operation for preventing the incorrect operation.

3 OPERATIONAL ASSISTANCE SYSTEM

The operational assistance system which avoid the collision with the obstacles by the incorrect operation using the 3-DOF joystick is proposed in this study. The block diagram of the proposed assistance system is shown in Figure 4.

In the proposed assistance system, the servomotor with the current control mode is used. The reaction torque T is generated by the motor, and the reaction force F at the operation point is represented by dividing the reaction torque T by the length L of the operating lever. The operating lever is tilted depending on the error between the reaction force F and the force f by the operator. Here, J is the inertia moment about the tilting center to the operating lever, and θ is the tilting angle of the operating lever. The velocity of the transfer machine corresponds to the tilting angle θ of the operating lever. The reaction force F can be increased by increasing the virtual elastic force and the viscous resistance in the operational assistance system. Therefore, the PD control to the tilting angle θ is constructed for generating the elastic force and the viscous resistance. Since the PD gains correspond to the distance between the obstacles and the transfer object, the reaction forces are increased by approaching the transfer object to the obstacles. The reference force F^* is generated by the PD control, and transformed to the current command i through the function $\xi(F^*)$. The operational assistance system as shown in Figure 4 is constructed to each operational axis.

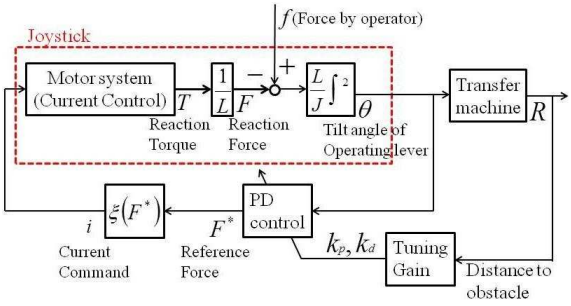

Figure 4: Block diagram of operational assistance system.

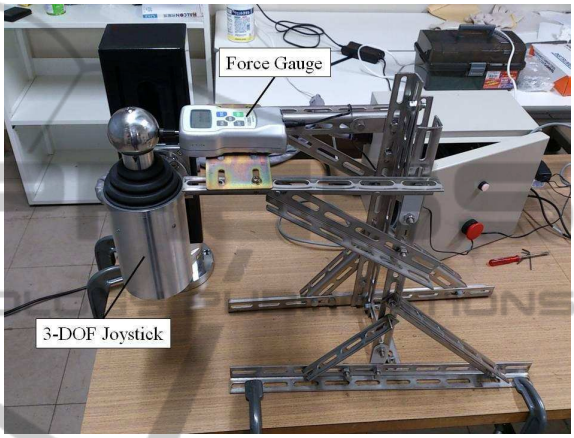

Figure 5: Measurement of reaction force using force gauge.

3.1 Transform Function between Current Command to Motor and Reaction Force

ξ shown in Figure 4 is the function between the reaction force and the current command to the motor. In design of the function ξ, the relation between the reaction force and the current command has to be clarified. Therefore, the reaction force at the operation point is measured by using the force gauge as shown in Figure 5. The measurement results are shown in Figure 6. In Figure 6, the markers are the reaction force measured by the force gauge. The reaction force cannot be displayed to the small current command. On the other hand, the reaction force to the current command over 0.3[A] is increased linearly to the current command. The function ξ is designed by the inverse function to the measurement data in Figure 6. However, the inverse function cannot be uniqueness on the small current command. Therefore, the threshold is set at the reaction force 5[N], and the inverse function between the reaction force and the current command is represented as

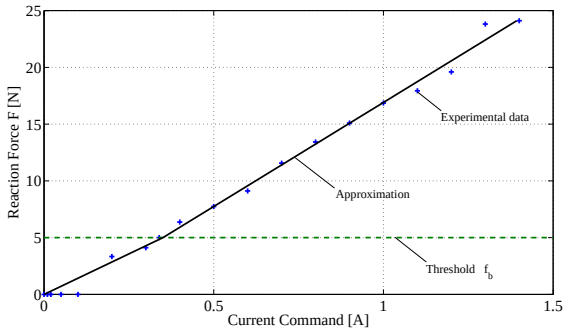

Figure 6: Relation between reaction force and current.

$$i = \begin{cases} i_a(F^*), & (F^* > f_b) \\ \frac{i_a(f_b)}{f_b} F^*, & (F^* \leq f_b), \end{cases} \quad (1)$$

where f_b is the threshold, and F^* is the reference force. i_a is linear approximation of the current command to the large reaction force. In this study, the function i_a is represented as

$$i_a(F^*) = \alpha_1 F^* + \alpha_0, \quad (2)$$

where $\alpha_0 = 51.81$ and $\alpha_1 = 56.04$.

3.2 Derivation Method of Shortest Distance between Obstacles and Transfer Object

The transfer object varies widely depending on the intended use. In the crane system, a long object such as a steel beam or a cylindrical container such as a liquid tank is transferred. Therefore, it is difficult to recognize the accurate geometry of the transfer object automatically. In this study, the transfer object is replaced by the ellipse including the transfer object as shown in Figure 7. Even the long object can be included reasonably by the ellipse. The ellipsoidal

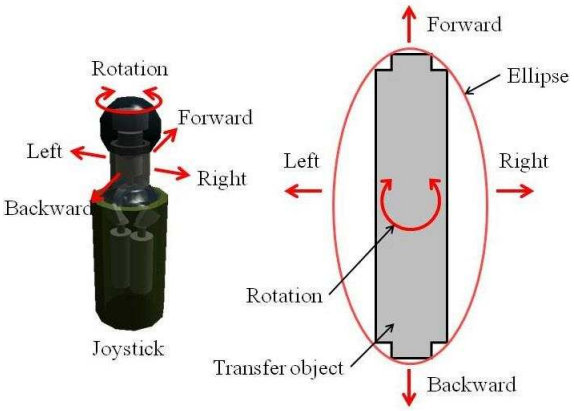

Figure 7: Transfer object included into ellipse and operational direction.

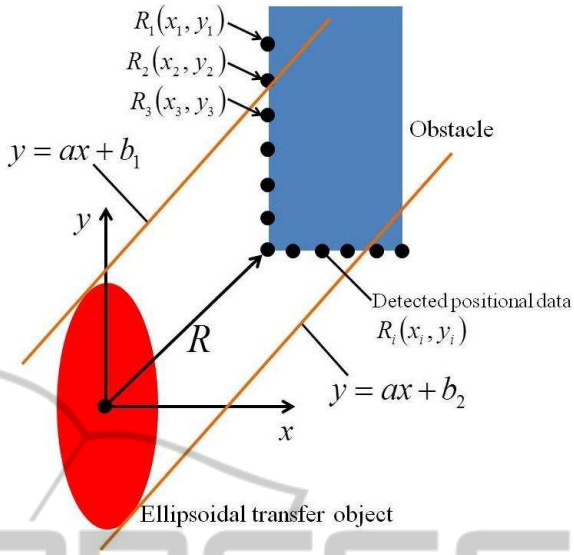

Figure 8: Positional relationship between ellipsoidal transfer object and obstacle.

transfer object needs the 3-DOF motion with back-and-forth, left-and-right, and rotation, and it can be manipulated by the proposed 3-DOF joystick.

In order to generate the reaction force for the obstacles avoidance, the shortest distance between the obstacles and the ellipsoidal transfer object is derived in this section. The relationship between the obstacle and the ellipsoidal transfer object is shown in Figure 8. In the operational assistance system as shown in Figure 1, the outline of the obstacles can be detected by a laser sensor. The shortest distance is selected from among the detected positional data, $R_i(x_i, y_i)$. At first in the derivation method of the shortest distance, the detected positional data on the transfer direction are picked up as

$$S_d = \{R_i(x_i, y_i) \in S | ax_i + b_1 < y_i < ax_i + b_2, \\ \mathrm{sgn}(x_i) = \mathrm{sgn}(\theta_x), \mathrm{sgn}(y_i) = \mathrm{sgn}(\theta_y)\}, \quad (3)$$

where S is the set of the detected positional data, and S_d is that on the transfer direction. θ_x and θ_y are the tilting angles of the operating lever on x- and y-axes, respectively. The linear functions $ax_i + b_1$ and $ax_i + b_2$ show the tangent lines to the ellipse which have same slope to the transfer direction of the transfer object. The slope a is represented as

$$a = \frac{\theta_y}{\theta_x}. \quad (4)$$

The intercept b_1 and b_2 can be derived from the tangent points of the tangent line and the ellipse. The distances $|R_{di}|$ of the detected positional data on the transfer direction are calculated as

$$|R_{di}| = \sqrt{x_i^2 + y_i^2}, \quad \forall R_{di} \in S_d. \quad (5)$$

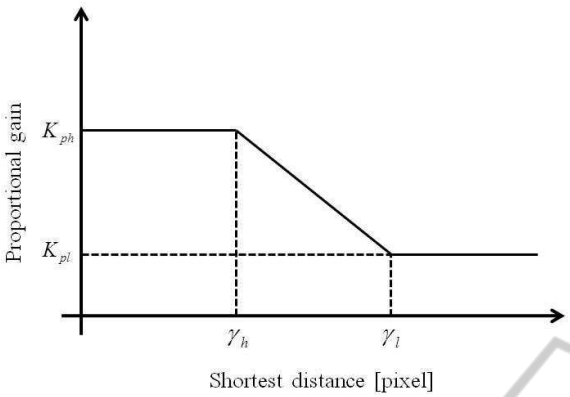

Figure 9: Relation between proportional gain and shortest distance.

The shortest distance $|R|_{\min}$ can be derived as

$$|R|_{\min} = \min|R_{di}|. \quad (6)$$

3.3 Design of Virtual Elastic Force

In the proposed operational assistance system shown in Figure 4, the reaction force can be represented as

$$J_i\ddot{\theta}_i + K_{di}\dot{\theta}_i + K_{pi}\theta_i = f_i L, \quad (7)$$

$$F_i^* = \frac{K_{di}}{L}\dot{\theta}_i + \frac{K_{pi}}{L}\theta_i, \quad i = x,y, \quad (8)$$

where F_i^* is the reference force on each axis, and K_{pi} and K_{di} are the proportional gain and the derivative gain on each axis, respectively. θ_i is the tilting angle of the operating lever on each axis. In the equation (8), $(K_{pi}/L)\theta_i$ is the virtual elastic force associated with the proportional gain. The reaction force is increased by increasing the tilting angle of the operating lever by the effect of the virtual elastic force. Then, the operating lever is pulled back to the original attitude by large proportional gain. Therefore, the joystick operation is constrained dynamically by changing the proportional gain. In order to avoid the obstacles, the relation between the proportional gain and the shortest distance $|R|_{\min}$ is represented as

$$K_{pi} = \begin{cases} K_{pil}, (|R|_{\min} > \gamma_l) \\ \frac{K_{pil}-K_{pih}}{\gamma_l-\gamma_h}(|R|_{\min} - \gamma_h) + K_{pih}, \\ \qquad (\gamma_h < |R|_{\min} \le \gamma_l) \\ K_{pih}, (|R|_{\min} \le \gamma_h), \qquad i = x,y, \end{cases} \quad (9)$$

where K_{pil} is the small proportional gain when the transfer object is far away from the obstacles. K_{pih} is the large proportional gain when the transfer object is close to the obstacles. γ_l and γ_h are the thresholds as shown in Figure 9. The thresholds have to be satisfied

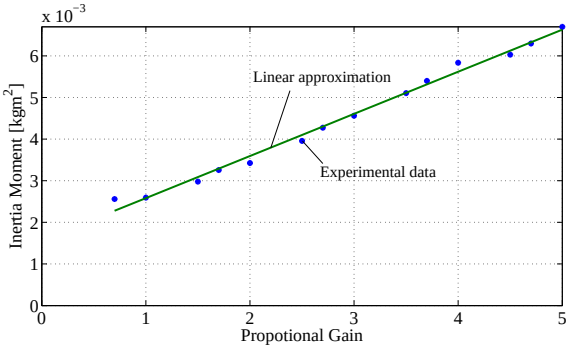

Figure 10: Relation between inertia moment and gain.

the following condition.

$$\gamma < \gamma_h < \gamma_l, \quad (10)$$

where γ is the long axis of the ellipsoidal transfer object.

3.4 Design of Virtual Viscous Resistance

As seen from the equation (7), the motion of the operating lever without the viscous resistance $(K_{di}/L)\dot{\theta}_i$ is the undamped vibration. Therefore, the virtual viscous resistance associated with the derivative gain K_{di} is designed for suppressing the vibration. Firstly, the undamped natural frequency ω_n can be obtained by the free vibration of the operating lever which is occurred by $K_{di} = 0$. Then, the inertia moment J is derived as

$$J = \frac{\omega_n^2}{K_{pi}}, \quad i = x,y. \quad (11)$$

The inertia moment obtained from the above procedure is shown in Figure 10. In this figure, the inertia moment is increased with increasing the proportional gain. The backlash of the bevel gear and the reducer is regarded as the cause of varying inertia moment. In order to design the derivative gain, the relation between the inertia moment and the proportional gain is represented by the linear approximation as

$$J^{(K_{pi})} = \beta_1 K_{pi} + \beta_2, \quad i = x,y. \quad (12)$$

In this study, β_1 and β_2 are given as 1.012×10^{-3} and 1.570×10^{-3}, respectively.

Using the inertia moment and the proportional gain, the derivative gain can be derived as

$$K_{di} = 2\zeta\sqrt{K_{pi}J(K_{pi})}, \quad i = x,y, \quad (13)$$

where ζ is the damping ratio. The damping ratio should be $\zeta = 1$ for realizing the critical damping, theoretically. However, the noise in the detected angular velocity of the operating lever is amplified by high derivative gain, and the motion of the operating

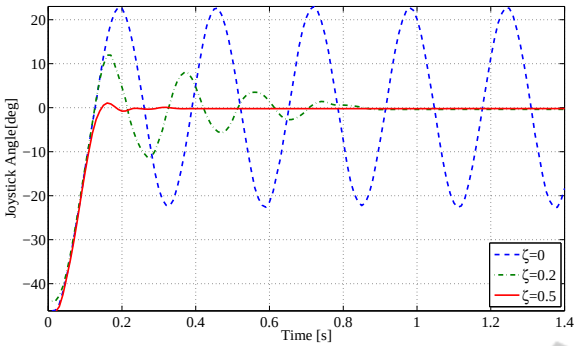

Figure 11: Experimental results to motion of operating lever depended on damping ratio.

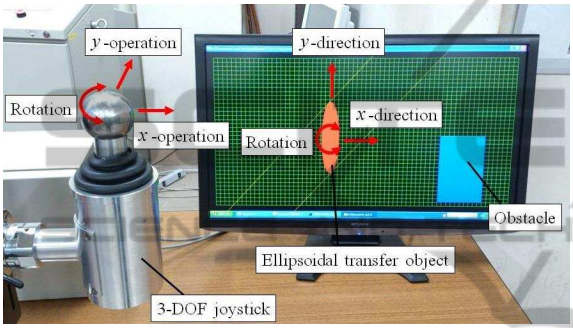

Figure 12: Photo of simulator of transfer machine manipulated by 3-DOF joystick.

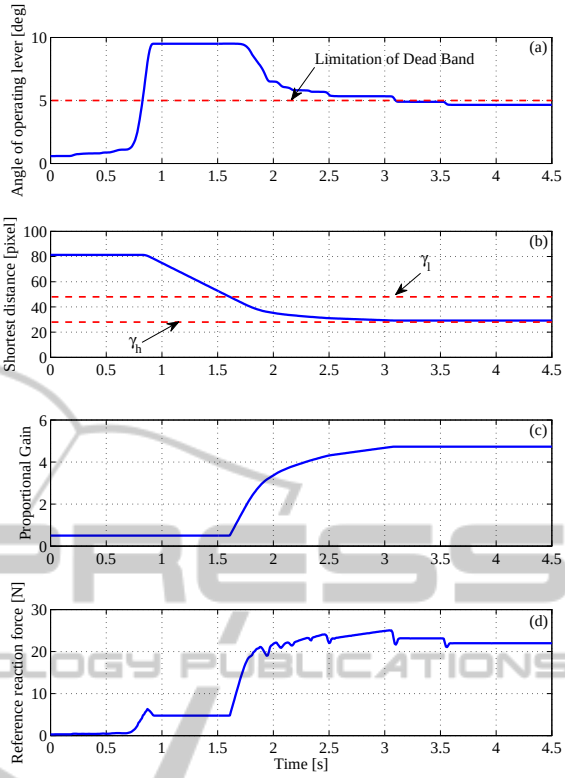

Figure 13: Experimental results to operation on *x*-axis.

lever is in unstable. The damping ratio is adjusted in the range of the damping vibration. In this study, the damping ratio was determined as $\zeta = 0.5$. The experimental results to the motion of the operating lever depended on the damping ratio are shown in Figure 11. It can be seen that the vibration is suppressed by the damping ratio $\zeta = 0.5$.

4 EXPERIMENTAL VALIDATION

The effectiveness of the proposed operational assistance system is verified by the experiments using the simulator of the transfer machine manipulated by the 3-DOF joystick. The simulator is shown in Figure 12. The long and short axes of the ellipsoidal transfer object are 18(pixel) and 4(pixel), respectively. The thresholds γ_l and γ_h for changing the proportional gain are given as 48(pixel) and 28(pixel). The low and high proportional gains are $K_{pxl} = K_{pyl} = 0.5$ and $K_{pxh} = K_{pyh} = 5.0$, respectively. The threshold γ_h is larger than the long axis of the ellipsoidal transfer object. Therefore, the joystick operation is constrained before the obstacle. In order to prevent the motion of transfer object influenced by the fluctuating hand of operator, we set up the dead band between the tilting angle of the operating lever and the command input to the transfer object. In this study, the dead band is with in ± 5[deg] of the angle of the operating lever.

In the experiments, the transfer object is approached to the obstacle by manipulating the joystick. The experimental results to the operations on *x*- and *y*- axes are shown in Figures 13 and 14, respectively. In these figures, (a) and (b) show the tilting angle of the operating lever and the shortest distance $|R|_{\min}$, respectively. (c) and (d) are the proportional gain K_p and the reference reaction force F^*, respectively. We assume the reference reaction force as the actual reaction force displayed on the top of the joystick. In figures (a), the broken line shows the limitation of the dead band which the transfer object does not work on the tilting angle of the operating lever within ± 5[deg]. In figures (b), the broken lines show the thresholds for changing the proportional gains. As seen from these figures, the reaction force is increased by approaching the obstacle, and the operating lever is pulled back to the vertical posture. The tilting angle of the operating lever is within the dead band, which is 5[deg]. Then, the transfer object can be stopped before the object as shown in Figures 13 (b) and 14 (b). Therefore, the collision avoidance to the obstacle is realized by the proposed operational assistance system.

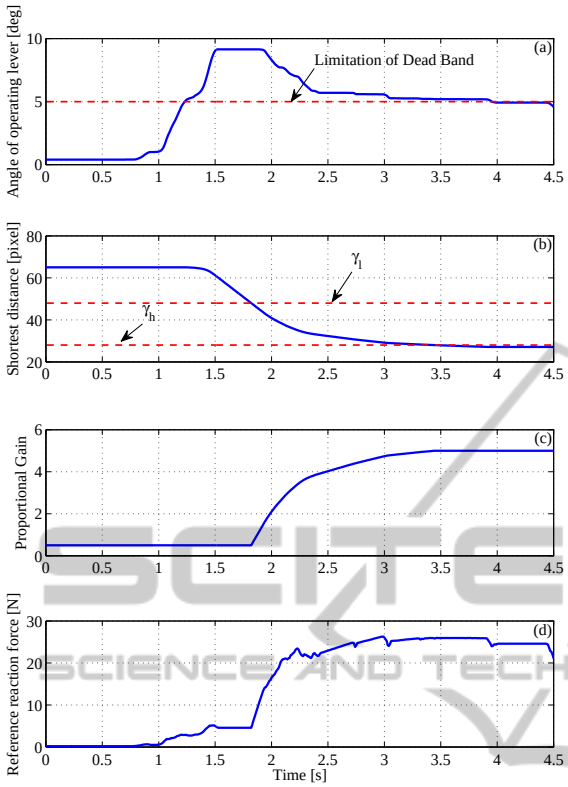

Figure 14: Experimental results to operation on *y*-axis.

5 CONCLUSIONS

The 3-DOF joystick with reaction force display has been proposed in this study. The joystick enables the operator to manipulate intuitively the 3-DOF transfer object on a plane. Furthermore, the operational assistance system for avoiding the collision with the obstacles has also proposed by using the 3-DOF joystick. The experiments using the simulator of the 3-DOF transfer object manipulated by the 3-DOF joystick shows that the proposed operational assistance system was effective.

In the future works, we will apply the operational assistance system to the actual transfer machine such as the crane system.

REFERENCES

Sawodny, O., Aschemann, H., and Lahres, S., ”An automated gantry crane as a large workspace robot”, Control Engineering Practice 10, pp.1323 - 1338, 2002.

Osumi, H., Kubo, M., Yano, S., and Saito, K., ”Development of tele-operation system for a crane without overshoot in positioning”, Proceedings of 2010 IEEE/RSJ International Conference on Intelligent Robots and Systems, pp.5799 - 5805, 2010.

Japan Crane Association, http://www.cranenet.or.jp/, 2011.

Yoneda, M., Arai, F., Fukuda, T., and Miyata, K., ”Assistance system for crane operation with haptic display operational assistance to suppress round payload awing”, Proceedings of International Conference on Control, Robotics and Automation, pp.2923 - 2929, 1999.

Yi-Chen, C., Hung-Lin, C., Shin-Chung, K., and Shang-Hsien, H., ”A smart crane operations assistance system using augmented reality technology”, Proceedings of 28th International Symposium on Automation and Robotics in Construction, pp.643 - 649, 2011.

Sato, R., Noda, Y., Miyoshi, T., Terashima, K., Kakihara, K., Nie, Y., and Funato, K., ”Operational support control by haptic joystick considering load sway suppression and obstacle avoidance for intelligent crane”, Proceedings of Annual Conference of the IEEE Industrial Electronics Society, pp.2321 - 2327, 2009.

Noda, Y., Kawaguchi, A., and Terashima, K., ”A mechatronics vision for smart wheelchairs”, Mobile Robots Navigation, Intech, pp.609 - 628, 2010.